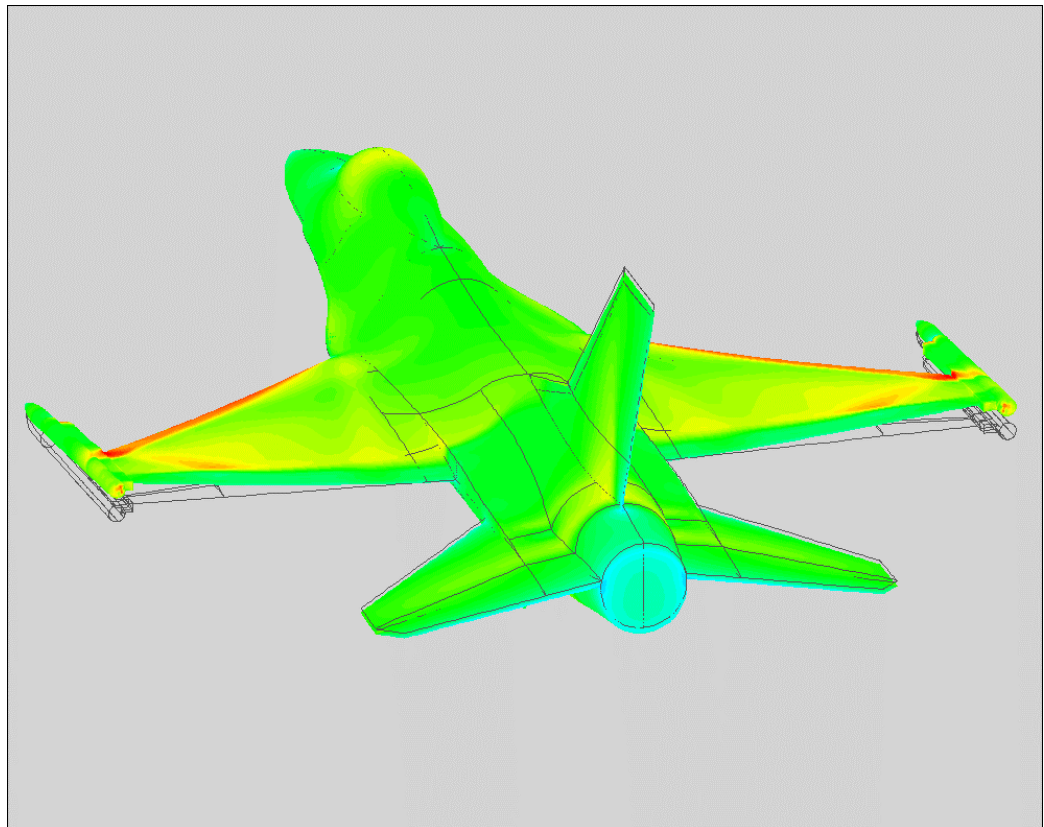NLR-TP-2001-346

Static aeroelastic simulation of military aircraft configuration in transonic flow

B.B. Prananta, I W. Tjatra, S.P. Spekreijse, J.C. Kok and J.J. Meijer

Nationaal Lucht- en Ruimtevaartlaboratorium

National Aerospace Laboratory NLR

NLR-TP-2001-346

Static aeroelastic simulation of military aircraft configuration in transonic flow

B.B. Prananta, I W. Tjatra, S.P. Spekreijse, J.C. Kok and J.J. Meijer

Division:	Fluid Dynamcis
Issued:	August 2001
Classification of title:	unclassified

Summary

INTRODUCTION: The research presented in this report is part of the AESIM-MIL project. The AESIM-MIL project aims at improving NLR support to the Royal Netherlands Air Force (RNLAF) in the field of aircraft vibration and aeroelaticity. The available methods is not adequate to analyse nonlinear aeroelastic phenomena occur during the F-16 flight test of RNLAF. These phenomena, especially limit cycle oscillations (LCO), need special attention because they pose a limit to the flight envelope for certain configurations and bring consequences to the aircraft maintenance. In the AESIM-MIL project knowledge and tools in nonlinear aeroelasticity are developed.

CONTENT OF THE WORK: This report describes a method developed in the AESIM-MIL project for static aeroelastic simulation of complete military aircraft configurations taking into account the nonlinear characteristics of transonic flow phenomena (shock waves, flow separation). The objectives are twofold:

1. The method developed in this research will be used primarily to provide a nonlinear statically deformed state which is one of the prerequisites for an accurate simulation of the dynamic state, e.g. flutter and LCO.
2. The method can also be used for accurate computation of aerodynamic forces at high-load conditions at which the interaction with the structural deformation is significant. These load data are important inputs for the design of maintenance scheduling and for fatigue life consumption analysis.

RESULTS: A method for the simulation of static aeroelastic behavior of fighter type aircraft has been developed. The coupled structural and aerodynamic system is represented by a nonlinear system of differential equations: the Euler/Reynolds-Averaged Navier-Stokes equations and linear structural equations of motion in the physical coordinates. The governing equations of the system are solved using an iterative method. To accommodate the incompatible representations of the fluid/structure interface by the aerodynamic and structural domain, two fluid-structure interpolation methods are employed: a surface spline interpolation method for a planar structural data and a volume spline interpolation for a genuinely three-dimensional structural data. The aerodynamic equations are solved on a multi-block structured grid using the multi-grid Runge-Kutta relaxation method. The solution algorithm of the flow equations is coupled with a robust, simple and computationally efficient multi-block grid deformation technique which is required for the adaptation of the multi-block grid points to follow the deformation of the fluid/structure interface. Results of the proposed method for the validation case of a restrained AGARD wing 445.6 compare very well with those obtained using MSC.NASTRAN. Relatively little fluid/structure interactions are required to obtain converged solutions. Subsequently, one of the NASA Dryden cases, i.e. a free-flying

F-16 configuration with tip missiles, was simulated and compared with NASA's computations and flight test. Satisfactory results are obtained. Trim iterations on the angle of attack, to reach the required lift coefficient for the specified g-level, were converged as quick as the fluid/structure iterations.

CONCLUSIONS AND FURTHER PLAN: The proposed method for the simulation of static aeroelastic analysis has been successfully validated for simple and complex geometry. Hereby, the objectives of the research are achieved. In the AESIM-MIL project the method will be further extended for time accurate simulations, which will enable dynamic aeroelastic simulations such as flutter and LCO for military aircraft configurations. The tools developed in this research are also exploited in other projects for static aeroelastic analyses at even higher load cases, compared to those considered in this report, in which a viscous flow modeling has been found necessary.

Contents

18 Figures

(37 pages in total)

List of symbols

Symbols

a	structural flexibility matrix also known as structural influence coefficient (SIC)
$\boldsymbol{B}$	vector of body force
$\boldsymbol{C}_{\mathsf{A}}$	coefficient of aerodynamic force
C_L	lift coefficient
C_M	moment coefficient
$\boldsymbol{g}$	vector of gravitational constant, $[n_{\mathsf{x}}, n_{\mathsf{y}}, n_{\mathsf{z}}]^T g$
$\boldsymbol{h}$	displacement vector
M	mass matrix
m	generalized mass, $\phi^T M \phi$
m_{ref}	reference mass
n	load factor, $1 + a_{\mathsf{z}}/g$
U	reduced velocity, $u_\infty / (\omega_{\mathsf{ref}} L_{\mathsf{ref}})$
V^*	speed index, $U/\sqrt{\mu}$
$\boldsymbol{x}$	physical coordinate vector
$\ddot{\boldsymbol{y}}$	acceleration at a structural point
v_{ref}	reference volume
α	angle of attack
δ_{F}	flap deflection
η	underrelaxation factor
ω_{ref}	reference frequency,
μ	mass ratio,
ρ_∞	mass density of air.

Sub/super-scripts

FF	free-free condition
stc	static condition
p	iteration counter
L	flexible part
R	rigid body part

1 Introduction

The research presented in this report is part of the AESIM-MIL project. The AESIM-MIL project aims at the development of knowledge and tools in nonlinear aeroelasticity to support the Royal Netherlands Air Force in operating advanced fighter aircraft, like e.g. F-16. Nonlinear aeroelastic phenomena, especially limit cycle oscillations (LCO), need special attention because they pose a limit to the flight envelope for certain configurations and bring consequences to the aircraft maintenance.

In the AESIM-MIL project an aeroelastic simulation method based on the Euler/Navier-Stokes flow modeling is developed. One of the consequences in using a nonlinear flow modeling is the dependency of the dynamic state to the static state[1]. To carry out a dynamic aeroelastic simulation properly, the dependency of the dynamic part to the the static part of the solutions has to be taken into account. One approach is to treat the static and dynamic parts as one system of equations. This approach usually leads to a method which is not optimal for either a static aeroelastic simulation or a dynamic aeroelastic simulation. The approach taken in the AESIM-MIL project is by starting a dynamic aeroelastic simulation from a converged static aeroelastic result. If necessary the static part is residualized in the dynamic aeroelastic simulation.

This report describes a method developed in the AESIM-MIL project for static aeroelastic simulations of complete military aircraft configurations taking into account the nonlinear characteristics of transonic flow phenomena (e.g. shock waves, flow separation, etc.). The method developed in this research will be used primarily to provide a nonlinear statically deformed state which is one of the prerequisites for an accurate simulation of the dynamic state, e.g. flutter and LCO. In addition, the method will also be used for accurate computation of aerodynamic forces at high-load conditions at which the interaction with the structural deformation is significant. These load data are important inputs for the design of maintenance scheduling and for fatigue life consumption analysis.

In static aeroelasticity, elastic deformation of a flexible structure causes a change in the pressure distribution on the surface of the structure. At the same time, a change in the surface pressure distribution brings a change in the structural deformation. The interaction between the aerodynamic and the elastic forces becomes more significant with the increase of the aerodynamic loads and the flow velocity. Special consideration has to be given to flows with large angle of attack and flows in the transonic regime due to the presence of shock wave and/or flow separations. In these kind

---

[1]This is not the case when the model is linear, e.g. using doublet-lattice method, in which the static and dynamic aeroelastic analyses may be carried out independently.

of flows, the characteristics of the aerodynamic loads are nonlinear with respect to the structural deformation. As a consequence, the fluid-structure interaction behavior in these aerodynamically nonlinear system will also be nonlinear.

In the conventional approach, the static aeroelastic simulation of an elastic structure couples the aerodynamic loads derived from a linearized aerodynamic theory, such as a panel method, with a linear or nonlinear structural finite element model 1, 16. For flows in the transonic speed regime, the aerodynamic nonlinearities are usually taken into account by explicitly combining the nonlinear aerodynamic data on a rigid structure (obtained from e.g. wind tunnel measurements) with the aerodynamic loads derived from a linearized aerodynamic method. However, for high performance military aircraft in which the flight maneuvers include those with high angle of attack and large deflection of control surfaces, this approach is unable to give an accurate prediction of the aerodynamic loads along with the corresponding structural deformation. A simulation method with more accurate flow representation is required, such as simulation based on the Euler/Navier-Stokes equations.

In the past, aeroelastic simulations of complete aircraft involving the nonlinear Euler/Navier-Stokes equations were considered impractical due to several reasons: the strong incompatibility between the aerodynamic grid and the structural grid which requires a sophisticated fluid/structure interpolation, the complexity of the grid generation and the subsequent grid adaptation when the surface deformed, the long computation time of the simulation, etc. However, recent developments in computational methods as well as in computer technology make the integration of an advanced computational fluid dynamic (CFD) method based on the solutions of the Euler/Navier-Stokes equations into an aeroelastic simulation system becoming feasible.

Several aeroelastic simulation methods based on the Euler/Navier-Stokes flow equations have been developed in the last decade, e.g. references 5, 10, 11, 15. These developments are usually started from well established CFD methods and concentrated on the fluid/structure coupling and the grid deformation aspects. In reference 5 the fluid/structure coupling employs a bi-linear interpolation on a virtual-surface interfacing the surface grids of the fluid and structural domain. The grid deformation employs a simple grid shearing method. The method of 5 has been mostly applied for simple configurations. The development at DASA-M follows the technique of virtual-surface5 but employs a finite-element type interpolation, the so-called neutral interface15. The multi-block grid deformation of 15 employs a combination of an unstructured Poisson algorithm and a transfinite-interpolation method. In the recent work published by Love et al. [10], the fluid/structure coupling employs NURBS surfaces. The Cartesian aerodynamic grid used in 10, however, can not be

deformed but instead are generated and destroyed according to the motion of the surface and also adapted to the expected flow features.

In this research, the ENFLOW system of NLR is extended to enable static aeroelastic simulation of complete military aircraft configurations. Learning from the literature and from the in-house development of a similar aeroelastic simulation method employing a full-potential flow modeling 6, the techniques to be employed in the extension of ENFLOW system have been identified. Fluid/structure interpolation is carried out using the superior volume-spline method of Hounjet and Meijer [7] which is capable of handling genuinely three-dimensional data. Aerodynamic grid deformation is carried out during the simulation using a robust and computationally efficient grid deformation algorithm which is based on a combination of volume-spline method and a transfinite interpolation.

The applications of the method for the AGARD 445.6 wing restrained at the tunnel wall and for a free-flying F-16 aircraft with wing tip missiles and the corresponding missile launchers are presented. For the first case comparisons are provided by MSC.NASTRAN. Very good agreement is obtained. For the F-16 case, one of the NASA Dryden case presented by Lokos et al. [9] is simulated. Satisfactory results have also been obtained.

Based on the presented results it may be concluded that the proposed method renders adequate accuracy and efficiency for static aeroelastic simulations. Applicability for very complex geometry, typical for fighter-aircraft configurations, has also been demonstrated. Hereby, the objectives of the research are achieved. The method will be further extended for time accurate simulation using the present results as the basis. This will enable dynamic aeroelastic simulations such as flutter and LCO for complex military aircraft configurations.

In the subsequent chapters, the governing equations and the global approach are described, followed by the discussions concerning the structural elasto-mechanical data and the aerodynamic solution. The grid deformation technique is then explained followed by some applications. Finally some concluding remarks are given.

2 Governing Equations and Global Approach

Simulation of the static aeroelastic deformation of a structure at a certain flight altitude is started from a zero-displacement state, also known as the jig state. Following the finite element (FEM) formulation for dynamical systems, the dimensionless matrix form of the governing equations for static deformation of a structure in physical coordinate system is given by

$$\boldsymbol{h} = a\,[\frac{1}{2}V^{*\,2}\boldsymbol{C}_{\mathsf{A}} + \boldsymbol{B}], \tag{1}$$

where $\boldsymbol{h}$ represents the static displacement vector corresponding to the structural degree of freedom (DOF), a represents the structural flexibility matrix ($a = K^{-1}$, with K is the structural stiffness matrix), C_{A} and $\boldsymbol{B}$ are vectors of the aerodynamic force coefficients and body force, respectively. V^* is called speed index and is defined as 3

$$V^* = \frac{U}{\sqrt{\mu}}, \tag{2}$$

in which $U = u_\infty/(\omega_{\mathsf{ref}}L_{\mathsf{ref}})$ and $\mu = m_{\mathsf{ref}}/(\rho_\infty v_{\mathsf{ref}})$ are the reduced velocity and mass ratio, respectively. The nondimensionalization has been selected to be consistent with the dynamic simulation (e.g. a frequency parameter ω is involved).

The vector of body forces consist of inertial forces due to gravity and due to aircraft acceleration given by the following equation

$$\boldsymbol{B} = M(\boldsymbol{g} - \ddot{\boldsymbol{y}}), \tag{3}$$

where M is the structural mass matrix, $\boldsymbol{g}$ is the vector of gravitational acceleration (assumed constant), and $\ddot{\boldsymbol{y}}$ is the vector of acceleration at the nodal point. All variables in equation (3) are given in non-dimensional form.

For a simulation at free flying condition, the inertial and aerodynamic forces at any moment have to be in balance. In this case, the effect of the inertial force due to the acceleration can be directly taken into account by modifying the aerodynamic force with the balancing inertial force or more conveniently it can be done by defining the so-called free-free (unconstrained) flexibility matrix 13 incorporating the structural rigid body modes to provide the inertial force and ensure the constant position of the center of gravity:

$$\boldsymbol{h} = a_{\mathsf{FF}}\,\frac{1}{2}V^{*\,2}\boldsymbol{C}_{\mathsf{A}}. \tag{4}$$

The free-free flexibility matrix in this equation is defined as $a_{\mathsf{FF}} = \mathcal{R}a\mathcal{R}^T$, in which $\mathcal{R}$ is the so-called rigid body modifying matrix. The static deformation equation is solved using an iterative

method for which the equation is cast in the following form

$$h_{\mathsf{stc}}^{p+1} = (1 - \eta)\, \boldsymbol{h}^p{}_{\mathsf{stc}} + \eta\, a_{\mathsf{FF}}\, \frac{1}{2} V^{*\,2} \boldsymbol{C}_{\mathsf{A}}. \tag{5}$$

In this equation, $\boldsymbol{h}^p$ represents the approximation of $\boldsymbol{h}$ during the p-th iteration. The structural state can then be updated as

$$\boldsymbol{x}^p = \boldsymbol{x}_{\mathsf{jig}} + \boldsymbol{h}_{\mathsf{stc}}^p, \tag{6}$$

where $\boldsymbol{x}_{\mathsf{jig}}$ is the structural position at zero-displacement state and $\boldsymbol{h}_{\mathsf{stc}}$ is the static deformation of the structure due to the total loads. An under-relaxation coefficient, η, is introduced to obtain a stable convergence to the final statically-deformed state.

For a restrained structure the support point provides the reaction forces and moments to balance the forces and moments acting on the structure. The reaction forces and moments vary with the given angle of attack and other parameters.

During a free-flight, however, support points can not be defined. Instead of providing reaction forces and moments, a configuration has to be sought which gives a balanced (trimmed) condition between the aerodynamic force and the inertial force. In the present study the balanced/trimmed condition is computed by defining target forces (or force coefficients) along with the trim variables. For example the necessary C_L^{target} can be defined to balance the inertial force due to the gravity and acceleration and pitching moment C_M^{target} about the aircraft center of gravity is required to be zero. The trim variables for this case are α and flap deflection δ_{F}. The following trim equations can then be defined:

$$\left\{ \begin{array}{c} C_L(\alpha, \delta_{\mathsf{F}}) - C_L^{\mathsf{target}} \\ C_M(\alpha, \delta_{\mathsf{F}}) - C_M^{\mathsf{target}} \end{array} \right\} = 0, \tag{7}$$

to be solved for the trim variables $[\alpha, \delta_{\mathsf{F}}]^T$. Starting from a given initial state, the trim variables $[\alpha, \delta_{\mathsf{F}}]^T$ are updated in a sequence as:

$$\left\{ \begin{array}{c} \alpha \\ \delta_{\mathsf{F}} \end{array} \right\}^{p+1} = \left\{ \begin{array}{c} \alpha \\ \delta_{\mathsf{F}} \end{array} \right\}^p - \eta \left[\begin{array}{cc} \partial C_L/\partial\alpha & \partial C_L/\partial\delta_{\mathsf{F}} \\ \partial C_M/\partial\alpha & \partial C_M/\partial\delta_{\mathsf{F}} \end{array} \right]^{-1} \left\{ \begin{array}{c} C_L(\alpha, \delta_{\mathsf{F}}) - C_L^{\mathsf{target}} \\ C_M(\alpha, \delta_{\mathsf{F}}) - C_M^{\mathsf{target}} \end{array} \right\} \tag{8}$$

where again η is an under-relaxation factor to ensure numerical stability. Note that the gradients of the target force coefficients to the trim variables have to be estimated prior to the simulation. If necessary these gradients can be updated during the simulation.

During static aeroelastic simulations the surface update due to structural deformation and trim analysis are carried out in each iteration. However, the structural deformation and trim correction are computed independently. So far, the experiences learned from the applications of the method show that the coupling turned out to be weak which allows the exclusion of the cross-terms.

3 Structural Dynamic Characteristics

As described in the previous chapter, the required elastomechanical data for a static aeroelastic analysis are:

  - flexibility data to determine the deflection of the structure,
  - mass data to determine the inertial load acting on the structure.

These data are also known to determine the dynamic characteristics of a structure. In the present research, the required elastomechanical data are obtained through a finite element modeling. Thus, the continuous structure is represented by a finite number of degrees of freedom (DOF's). The flexibility and mass data are then expressed as matrices. Finite element package MSC.NASTRAN is employed. Two configurations are considered in this report, the AGARD 445.6 wing and the F-16 aircraft with AMRAAM missiles and the corresponding missile launchers at the wing tip.

The structural properties of the AGARD 445.6 wing are represented by equivalent shell and plate elements (the CQUAD4 shell element with 24 DOF's). Figure 1 shows the finite elements model of the AGARD wing. To model the clamping at the tunnel wall, a large mass is attached to the root of the wing. To balance the construction statically a force of exactly the same magnitude as the total weight in the opposite direction to the gravity is given at the attachment point. This technique is called large-mass method, see reference 14.

To obtain the desired data, the MSC.NASTRAN is executed for normal mode analysis where at certain stages of the computation the mass and stiffness matrices are written as extra outputs. The commands to produce extra outputs are implemented using DMAP, see reference 2. Since a data extraction from MSC.NASTRAN using DMAP commands is not trivial a verification step was considered necessary. The verification proceeded by comparing the natural frequencies and mode shapes computed by NASTRAN and those obtained independently using the LAPACK numerical routine library with the input of the extracted mass and stiffness matrices. Identical results have been obtained which verifies the data extraction process. The desired flexibility matrix can then be obtained directly by inverting the stiffness matrix:

$$a_{\text{direct}} = K^{-1}. \tag{9}$$

Other method to obtain the flexibility matrix is by an expansion in the mode shapes, taking advantage of the characteristics of normal modes:

$$a_{\text{mode}} = \sum_{n=1}^{N^*} \frac{1}{m_n \omega_n^2} \phi_n \phi_n^T, \tag{10}$$

where m is the generalized mass, ω is the natural frequency, ϕ is a row matrix representing the mode shape and subscript n designates the mode number. When all modes are taken into account in the expansion, i.e. $N^* = N_{\mathsf{DOF}}$ where N_{DOF} is the number of DOF's available in the structural model, a_{direct} is recovered. When $N^* < N_{\mathsf{DOF}}$ the resulting flexibility matrix a_{mode} is only an approximation to a_{direct}. In the present study the first method, i.e. equation (9), is always used except when otherwise is mentioned.

Structural properties of F-16 configuration are represented by a combination of shell/plate elements (CQUAD4) with beam (CBEAM) and bar (CBAR) elements, see Figure 2. A symmetrical free-flight configuration is modeled by putting constraints along the fuselage and defining the rigid body degrees of freedom (using SUPORT command) of normal translation and pitching rotation. After a normal mode analysis using NASTRAN the so-called free-free mode shapes are obtained along with free-free stiffness and mass matrices as extra outputs. Note that a free-free stiffness matrix can not be inverted directly. First, the DOF's at the point where the rigid body modes are defined (SUPORT point), is removed to obtain a restrained stiffness matrix. The restrained stiffness matrix can then be inverted straightforwardly to obtain restrained flexibility matrix. Subsequently, the necessary modification, based on the DOF's at the SUPORT point, is applied to the restrained flexibility matrix to obtain a free-free flexibility matrix, see reference 12 for more detail description:

$$a_{\mathsf{direct}} = \mathcal{R} K_{\mathsf{restrained}}^{-1} \mathcal{R}^T, \tag{11}$$

where $K_{\mathsf{restrained}}$ is the restrained part of the K matrix and $\mathcal{R}$ is the rigid body modifying matrix. For a free-free condition, the technique using mode shape expansion becomes:

$$a_{\mathsf{mode}} = \sum_{n=N_{\mathsf{R}}+1}^{N^*} \frac{1}{m_n \omega_n^2} \phi_n \phi_n^T, \tag{12}$$

where N_{R} is the number of rigid DOF's. Note that the natural frequency of the rigid mode of the structure, i.e. without the aerodynamic forces, is zero.

4   Aerodynamic Solution

The development of the static aeroelastic simulation method described in this report is based on the application of the in-house developed CFD system called ENFLOW. The ENFLOW system has been extensively used for the prediction of aerodynamic forces on rigid configurations. This research enhances the ENFLOW system to include the interaction with the structure.

ENFLOW system consists of components which are necessary for a CFD analysis: tools for aerodynamic geometry processing, ENDOMO block decomposition tool, ENGRID grid generator, ENSOLV flow solver and ENADAP grid adaptation tool based on the flow solution, see e.g. reference 8. The flow solver ENSOLV, which is capable of solving the unsteady Euler/Reynolds-Averaged Navier-Stokes equations in a deforming multi-block domain, applies the Runge-Kutta time integration accelerated by local time stepping, implicit residual averaging and a multi grid scheme. To improve the accuracy in boundary layers, a modified matrix dissipation scheme by Swanson-Turkel was implemented. Turbulent flows are described by closing the Reynolds-averaged Navier-Stokes equations with one of the available turbulent models, which are algebraic models (Baldwin-Lomax, Cebeci-Smith and Johnson-King models) and two equations models ($k - \omega$ model). An important aspect of the flow solver is that it allows multi-block grids which are only C^0-continuous at the block interface, or even only partly continuous. These properties simplify the multi-block grids generation procedure (grid in each block can be generated independently once the grids at the block interfaces have been defined and the grid refinement process within a certain block is more efficient) and the multi-block grid adaptation process.

During the fluid/structure iteration the grid has to follow the deforming surface due to the aerodynamic and inertial load. This requires grid adaptation tools other than that based on the flow solution. A detailed description of the grid adaptation process for grid deformation will be given later in this report.

5 Fluid/Structure Interpolation

The iteration process to compute the structural static deformation is started with the computation of the flow field around the rigid baseline configuration resulting in aerodynamic loads at the aero-dynamic grid points which are then transfered to the structural grid. Then, the process is continued by a sequential computation of the structural deformation, the transformation of structural surface deformation into the aerodynamic grid, the aerodynamic grid deformation, the aerodynamic flow solution and the transformation of aerodynamic loads into the structural grid points, and so on. The schematic diagram of this iterative process is shown in Figure 3.

The fluid/structure interaction (data exchange) in this loosely-coupled method is carried out through the fluid/structure interface geometry of the structural and aerodynamic model. In most cases the geometry representation of the fluid/structure interface on the structural side and on the aerody-namic side are different. The differences may come from several factors, amongst other:

- Types of solution/discretization method: the structural equations are solved using a finite element method while the aerodynamic equations are solved using a finite volume method,
- Different requirement concerning the accuracy/grid density,
- Level of geometry modeling, e.g. for a thin wing the structural model would employ plate elements (or beam element for a high aspect ratio wing) while the aerodynamic model uses volumetric grids.

The differences in the fluid/structure geometry representation imply that a direct exchange of information between the aerodynamic and structural domains is impossible. A common way to solve domain incompatibility of this kind is to use a spline technique. The structural deformation on the fluid/structure interface side of the structure is represented by a spline function and apply the same function to also the fluid/structure interface on the aerodynamic side. Similarly, the distributed aerodynamic loads on the aerodynamic surface are represented by equivalent point loads at each of the structural grids.

The displacement vector in the aerodynamic grid, $\boldsymbol{h}_{\mathsf{aero}}$, can be expressed in terms of the dis-placement vector in the structural grid points, $\boldsymbol{h}_{\mathsf{struc}}$, as

$$\boldsymbol{h}_{\mathsf{aero}} = G\boldsymbol{h}_{\mathsf{struc}} \tag{13}$$

where G is the interpolation or spline matrix. Similarly, the point loads vector in structural grid, $\boldsymbol{F}_{\mathsf{struc}}$, can be written as

$$\boldsymbol{F}_{\mathsf{struc}} = G^* \boldsymbol{F}_{\mathsf{aero}} \tag{14}$$

where $\boldsymbol{F}_\text{aero}$ is the point loads vector at the aerodynamic grids. Relationship between the two spline matrices, G and G^*, is obtained by requiring that the data exchange between the two domains can be carried out without energy loses (energy conserving fluid-structure interpolation). This leads to matrix relation

$$G^* = G^T,$$ (15)

meaning that G^* may not be generated independently, instead the transpose of G should be used.

The spline matrix G itself is defined using a planar surface spline method or volume spline method. A detailed discussion on the numerical computation of G matrix can be found in reference 7.

6 Multi-Block Grid Adaptation Technique For Grid Deformation

One major difficulty in applying the Euler/Navier-Stokes solutions for aeroelastic computation is the aspect of updating the grid. Early developments, as reported in e.g. 4, uses simple shearing method which limits its application to simple topologies and small deformations. In the present research an efficient multi-block grid deformation method is developed which is relatively general, robust and applicable for large deformation.

Several requirements are put on the grid deformation method. Since the grid adaptation has to be carried out at each iteration step (once the fluid-structure interface is updated), it is of major importance to keep the method simple and efficient. Further, it should be robust, e.g. the grid may not fold during a simulation, and grid quality conserving, e.g. the initial clustering should be preserved.

A multi-block grid consists of a set of blocks $\{B\}$ with each block having its own structured three-dimensional volume grid, faces $\{F\}$ with each face having its own two-dimensional structured grid, edges $\{E\}$ with each edge having its own curved one-dimensional grid, and vertices $\{V\}$ which are defined by position vectors x_V.

In principle, a similar spline method applied for the interpolation of the surface deformation between structural grids and aerodynamic grid could also be used to interpolate the displacement on the surface grids into the grids in the field, provided that a three-dimensional spline method was employed. However, for an average-size grid with millions of points this would lead to an unacceptable long computation time. In this investigation, a computationally efficient grid adaptation technique is proposed. In this technique, the displacement of the vertices and edges of the multi-block grid is computed using a volume spline interpolation method based on the fluid-structural interface spline data. After that, the displacement of the faces and blocks are computed using transfinite interpolation (TFI) with a blending function defined by the initial grid.

By keeping the blending function constant during the grid deformation process, the grid quality should remain constant during the simulation. The TFI method for the calculation of the grid displacements in the interior of a face $\{F\}$, consist of two recursive steps which are: the calculation of the displacements in the interior by a straight-line interpolation in the i-direction, followed by a mismatch addition of the displacements along the second pair of the opposite edges by straight-line interpolation in the j-direction. Once the displacements of the faces $\{F\}$ calculated, the TFI method is applied to calculate the displacements in the interior of the blocks $\{B\}$.

For a block, beside the recursive two steps which are applied for the face interpolation, an additional step has to be carried out which is a mismatch addition of the displacements along the third pair of the opposite faces by straight-line interpolation in the k-direction. Using this TFI technique, displacement of only a small portion of the grid points is computed by the computationally expensive volume spline interpolation method, while the displacement of the larger part of the grid points is computed by the computationally inexpensive TFI technique. In case grid folding appears in the interior of some blocks, the interior grid of the folded block need to be recalculated using the original grid generation algorithm. The multi-block grid adaptation described in this section implemented into ENFLOW system in a module called DEFGRD.

7 Simulation Results

To demonstrate the accuracy of the proposed static aeroelastic simulation system, calculation of structural deformations on two configurations were carried out:

1. AGARD wing 445.6 weakened model No. 3 restrained at the tunnel wall. The flexibility and mass matrices are obtained using MSC.NASTRAN, see page 12. Two different flow conditions have been simulated:

   – Subsonic condition of $M_\infty = 0.45$, $\alpha = 2$ degrees and $q_\infty = 6372$ Pa,
   – Transonic condition of $M_\infty = 0.96$, $\alpha = 2$ degrees and $q_\infty = 2935$ Pa.

   These flow conditions have been taken from [17] and represent the flutter boundary at zero angle of attack. The results of the experiment show a transonic dip with the bottom at M_∞=0.96. Stand alone codes have been used for this case: ENSOLV flow solver in the Euler mode employing either a transpiration boundary condition or a grid deformation approach, DEFGRD grid deformation code and STCDEF static deformation code. Comparison are made with the static aeroelastic results of MSC.NASTRAN in which a vortex-lattice linear aerodynamic theory is used. Similar results are expected between ENSOLV and NASTRAN for the subsonic case where assumptions underlying the linear aerodynamic theory are valid. For the transonic case, however, some differences are expected.

2. A free-flying F-16 configuration equipped with wing tip missile and the corresponding missile launcher during a $5g$ pull-up maneuver at Mach number $M_\infty = 0.9$ and altitude $h = 5,000$ ft. The flexibility and mass matrices are also obtained using MSC.NASTRAN, see page 13. For the F-16 case, the static aeroelastic simulation is carried out using the new version of ENSOLV in which all the supporting modules, i.e. STCDEF and DEFGRD, have been incorporated into one code.

7.1 AGARD wing 445.6

The results of ENSOLV for the AGARD wing at the subsonic case and those of NASTRAN are presented in Figure 9. The total load acting on the wing consists of the aerodynamic load and the inertial load due to gravity (i.e. $1g$ load). Figure 9 shows both the results for which the transpiration boundary condition approach (upper figure) and the grid deformation approach (lower figure) was applied. The results of ENSOLV have been obtained after 20 fluid/structure iterations with an under-relaxation coefficient $\eta = 0.5$. During the first iteration 20 multigrid cycles of ENSOLV were applied and in the subsequent iteration, only 4 multigrid cycles were applied. The vertical deformation in these figures are normalized using the root chord length. The maximum deformation of 6.5% of the chord at the wing tip is observed. All results show good agreement.

Vertical deformation along the wing span is given in Figure 8. Both the leading edge and trailing edge deformations have a parabolic shape (similar to the deformation of a Timoshenko cantilever beam due to a point load at the end). It can be seen that results obtained using both the transpiration boundary condition and the grid deformation approach are in a very good agreement with MSC.NASTRAN results.

The lifting pressure (ΔCp) contours computed using MSC.NASTRAN vortex-lattice linear aerodynamic theory and ENSOLV are compared in Figure 10 which shows that in subsonic speed both methods give similar results. A detailed look at the surface pressure distribution along the wing chord at four different wing sections is presented in Figure 11. These are surface lifting pressure distribution at the final deformed shape of the wing. Both solutions provide almost identical surface pressure distributions. Since the free stream velocity is still in the subsonic regime (small nonlinearities in the flow fields), the vortex-lattice method can produce results which are as accurate as the results produced by the Euler solutions.

For the transonic case, although differences are expected, these should not be very large because the wing has a quite large sweep angle and a relatively thin cross section (maximum t/c is 5%), combined with small angle of attack. There are no shock in the flow field, as depicted in Figure 12 which shows sectional lifting pressure distribution at several span stations. Linear vortex-lattice solutions predict a lower lifting pressure in the region close to leading edge compared to the prediction using Euler equation employing both the transpiration boundary condition and the grid deformation approach. Differences are also expected between ENSOLV solutions employing the transpiration boundary condition with solutions employing grid deformation approach since the small perturbation assumption used in the transpiration boundary approach may be violated for this flow condition. A comparison is made for the final static vertical deformation along the wing span as depicted in Figure 13. Similar differences are observed as before between the two solutions but with slightly larger magnitude.

7.2   F-16 configuration

Static deformation of F-16 in various flight conditions and various store configurations have been investigated at NASA Dryden and presented by Lokos et al. [9]. The investigation was directed towards the pointing error of the AMRAAM missile due to the static deformation of the structure during a high-g maneuvering flight. Comparison was made between flight test data and computational results for several flight condition (Mach number, altitude and aircraft gross weight variations).

In the present work, one of the NASA Dryden static deformation cases is selected for the method validation, i.e. the F-16 configuration equipped with the advanced medium range air to air missile

(AMRAAM) at the wing tip during a 5-g symmetrical pull-up maneuver at an altitude of 5,000 feet. For this flight configuration, results in the form of front and rear spar deformation and twist angle distribution in the spanwise direction are available. It should be kept in mind however, that the present results may show some differences compared to the NASA Dryden's results because differences in the input data could not be avoided due to the unavailability of the same structural model and also due to the unavailability of some flight condition data. The computational results of reference 9 are obtained using a relatively high resolution FEM model of a symmetrical F-16 C/D block 40 aircraft with about 160,000 degree of freedoms. A given set of load cases was used. Meanwhile, computation in this work has been carried out using a simplified FEM model, suitable for flutter analysis, of a symmetrical F-16 A/B block 25 aircraft with about 1,000 DOFs. The total weight of the aircraft which was derived from the FEM model is 23,072 lbs, which is somewhat lower than the total weight given in reference 9 (24,600 lbs).

An aerodynamic grid has been generated for the computations of NASA Dryden case. Since a symmetric case is considered, only a half configuration of an F-16 is used. The grid consists of 310 blocks holding in total about 2 millions grid points. With inputs of the jig-surface CAD definition of the F-16 "Big-Tail" the blocks were arranged using ENDOMO domain modeler. The block boundaries of the whole computational domain are shown in Figure 4. It can be seen that the global topology is of HO type. The block boundaries at the symmetry plane, i.e. $y = 0$ plane, are presented in Figure 5 showing the details close to the aircraft surface.

After the domain is divided into blocks, the grid is generated using ENGRID by sequentially tuning the grid distribution on the edges, the faces and finally in the blocks. Unlike tuning a grid for a viscous flow analysis, where boundary layer has to be properly accommodated, less stringent requirements are posed to the distribution of Euler grid points close to solid surfaces. Leaving in the direction relatively normal to the surface with uniform distribution are preferred to achieve accurate variable extrapolation to the surface. For the Euler equations from the five flow variables only one variable may be specified on the solid surface, i.e. the normal velocity, the rests have to be extrapolated. A partial view of the grid on the symmetry plane and on the surface of the F-16 is shown in Figures 6 and 7.

The static aeroelastic simulation was carried out using the integrated version of ENSOLV which contains all necessary modules: the flow solver, the static deformation module, the trim analysis module and the grid deformer. The Euler model has been used in the flow solver. Computations were performed on both constrained and free flight conditions. For the constrained simulation, only the aerodynamic force is applied.

During a free-flight simulation, to match the g-level with the given one, i.e. $5g$, the aircraft attitude has to be trimmed. The trimming can be carried out by modifying the angle of attack and the control surface deflection in such away that all forces and moments on the aircraft are in balance. For F-16 aircraft the control surfaces are scheduled depending on various flight parameters, e.g. Mach number, angle of attack, static pressure, etc. In the present work only the angle of attack will be used as the trim variable to trim the lift and leaving the moments un-trimmed. Full trim analyses will be carried out in the future research.

The necessary C_L to produce the g-level corresponding to $5g$ can be computed from the mass data and the flight parameter data, which is C_L=0.385. This value was set as the target C_L for the trim analysis. Figure 14 shows the convergence history of the lift coefficients and the angle of attack correction ($\Delta\alpha$) with respect to the initial angle of attack. The calculation was started from a zero deformation condition at an initial $\alpha = 4.5$ degrees with a corresponding C_L of about 0.46. The target lift coefficient is reached in less than 30 iterations giving a trimmed alpha of 4.5-0.61 degrees.

The maximum/minimum vertical displacements convergence history is shown in Figure 15. It can be seen that a similar rate of convergence as that for trim analysis was obtained for the deformation. Surface pressure distribution at the converged state is shown in Figure 16. Spanwise bending (vertical) deflection of the front and rear spars for $5g$ maneuver is shown in Figure 17. Results from the present study compare well with both the numerical results and flight test data as reported in reference 9. The differences in the results may be attributed to the previously mentioned differences in modeling the F-16 configurations. The restrained condition gives, in general, results which are closer to the flight test data compared to the results obtained by imposing the free-free condition and also compared to the NASTRAN results of Lokos et al. [9]. One possible reason for this is that in the calculation with free-free condition the leading-edge and trailing-edge flap deflections are not simulated correctly because the flight test flap setting conditions are not reported in reference 9.

Wing box twist distribution, which is defined based on the difference between the front spar and rear spar deflection, is shown in Figure 18. As for the bending deflection, calculation with constrained condition predicts more accurate twist distribution compared to calculation with free-free condition.

8 Concluding Remarks

In this report a static aeroelastic simulation system ENFLOW is presented. The main objectives of developing the static aeroelastic simulation are: to provide an initial condition for a dynamic aeroelastic simulation and to enable accurate computation of aerodynamic forces at a high-load condition. The proposed method, which is solved using an iterative scheme, consists of the following components:

1. Robust Euler/Navier-Stokes flow solver employing a finite-volume method on structured multi-block grids,
2. Structural solver based on linear theory with the flexibility and mass data obtained from the widely used finite-element code MSC.NASTRAN,
3. Fluid/structure interpolation method employing planar surface spline and three-dimensional volume spline methods,
4. Grid deformation method combining the volume spline technique for the block edges and an efficient transfinite interpolation technique for the block faces and the grid points.

These components have been implemented in the new version of ENSOLV.

Numerical results are shown for AGARD 445.6 wing restrained at its root and a free-flying F-16 aircraft configuration with wing tip launchers and missiles. For subsonic case, very good agreement is obtained for the AGARD 445.6 wing between the results of ENSOLV in the Euler mode and those of MSC.NASTRAN. The latter uses a linear lifting surface theory. As expected, there are some differences between the results of ENSOLV and MSC.NASTRAN for the transonic case. However, the differences are small due to the small thickness ratio and large sweep angle of the AGARD 445.6 wing. The results for the F-16 are compared well with the results of NASA Dryden for a $5g$ pull-up maneuver. The $5g$ condition has been achieved by trimming the angle of attack to obtain the required lift coefficient.

Based on the results of the applications, it may be concluded that the applied fluid/structure iterative method is robust, accurate and efficient in term of quite rapid convergence. Current and future studies include the application of the newly developed method for even higher load conditions at which the Navier-Stokes mode is necessary and also for fully-loaded configurations at which both wing-tip missiles and underwing stores are present. At the moment, the development activities is focussed in the extension of this method for dynamic aeroelastic simulations.

ACKNOWLEDGEMENT

NLR

9 References

1. E. Albano and W.P. Rodden. A doublet-lattice method for calculating the lift distributions on oscillating surfaces in subsonic flow. *AIAA Journal*, 7(2):279–285, 1969.

2. D. Bella and M. Reymond. *MSC/NASTRAN DMAP Module Dictionary*. MacNeal-Schwendler Corporation, USA, 1995.

3. B.J.G. Eussen, M.H.L. Hounjet, J.J. Meijer, B.B. Prananta, and I W. Tjatra. Perspectives of NLR methods to predict wing/store flutter and dynamic loads of fighter-type aircraft. ICAS Paper 2000.461.1, ICAS, also NLR-TP-2000-447, NLR, 2000.

4. G.P. Guruswamy. Time accurate unsteady aerodynamics and aeroelastic calculations of wings using Euler equations. *AIAA Journal*, 28(3):641–649, 1990.

5. G.P. Guruswamy and C. Byun. Fluid-structural interactions using Navier-Stokes flow equations coupled with shell finite element structures. AIAA Paper 93-3087, AIAA, 1993.

6. M.H.L. Hounjet and B.J.G. Eussen. Outline and application of the NLR aeroelastic simulation method. In *Proceedings of 19th Congress of ICAS*, pages 1418–1441, Anaheim, 1994. ICAS, also NLR-TP-94422, NLR, 1994.

7. M.H.L. Hounjet and J.J. Meijer. Evaluation of Elastomechanical and Aerodynamic Data Transfer Methods for Non-planar Configurations in Computational Aeroelastic Analysis. In *Proceedings of 1995 CEAS International Forum on Aeroelasticity and Structural Dynamics*, pages 11.1–11.24, Manchester, 1995. Royal Aeronautical Society, also NLR-TP-95690, NLR, 1995.

8. J.C Kok, J.W. Boerstoel, A. Kassies, and S.P. Spekreijse. A robust multi-block navier-stokesflow solver for industrial applications. Report NLR-TP-960503, NLR, Paper presented at Third ECCOMAS Computational Fluid Dynamics Conference, Paris, 1996.

9. W.A. Lokos, C.M. Bahm, and R.A. Heinle. Determination of stores pointing error due to wing flexibility under flight load. Technical Memorandum TM 4646, NASA, 1995.

10. M. Love, T. De La Garza, E. Charlton, and D. Eagle. Computational aeroelasticity in high performance aircraft flight loads. ICAS Paper 2000.481.1, ICAS, 2000.

11. B.B. Prananta and M.H.L. Hounjet. Aeroelastic Simulation with Advanced CFD Methods in 2-D and 3-D Transonic Flow. In *Proceedings of 1996 Unsteady Aerodynamics Conference*, pages 7.1–7.14, London, 1996. Royal Aeronautical Society.

12. B.B. Prananta, J.C. Kok, S.P. Spekreijse, M.H.L. Hounjet, and I W. Tjatra. Aeroelastic simulation method for military aircraft configurations. Report NLR-CR-2000-626, NLR, 2000.

13. W.P. Rodden and E.H. Johnson. *MSC/NASTRAN Aeroelastic Analysis User's Guide*. MacNeal-Schwendler Corporation, USA, 1994.

14. G. Sitton. *MSC/NASTRAN Basic Dynamic Analysis User's Guide*. MacNeal-Schwendler Corporation, USA, 1993.

15. M. Stettner, W. Haase, A. Eberle, J. Grashof, and M. Schneider. Coupled static and dynamic aeroelastic simulations in transonic and supersonic flow. ICAS Paper 2000.482.1, ICAS, 2000.

16. F.A. Woodward. A unified approach to the analysis and design of wing-body combination at subsonic and supersonic speed. AIAA Paper 68-0055, AIAA, 1968.

17. E.C. Yates Jr., N.S. Land, and J.T. Foughner Jr. Measured and calculated subsonic and transonic flutter characteristics of a 45° sweptback wing planform in air and in Freon-12 in the Langley Transonic Dynamics Tunnel. Report TN-D-1616, NASA, 1963.

Figures
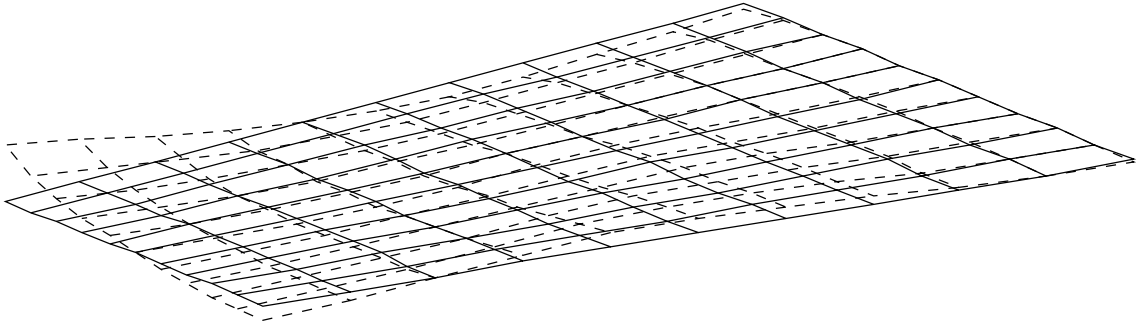
Fig. 1   Finite-element model of AGARD *445.6 wing consisting of* QUAD4 *elements, the dashed line shows the fourth flexible mode*
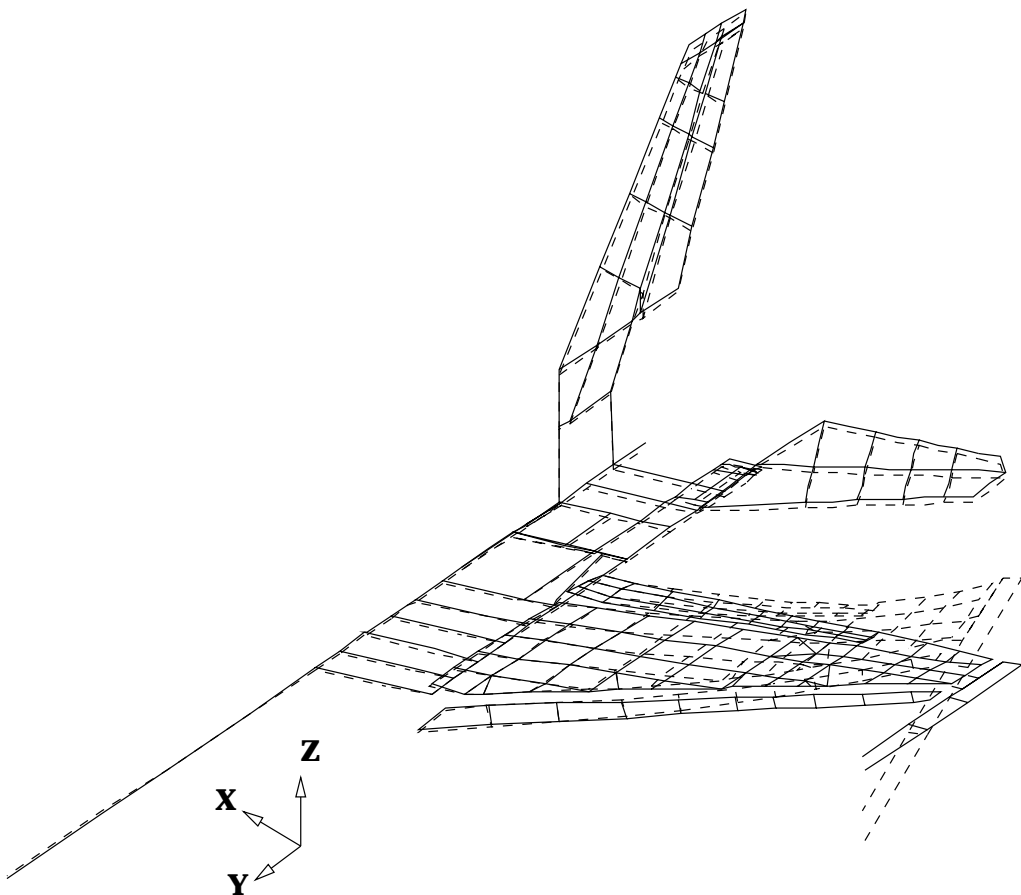
Fig. 2   Finite element model of F-16 *aircraft with tip missile consisting of* CBEAM *and* QUAD4 *elements, the dashed line shows the second flexible mode*
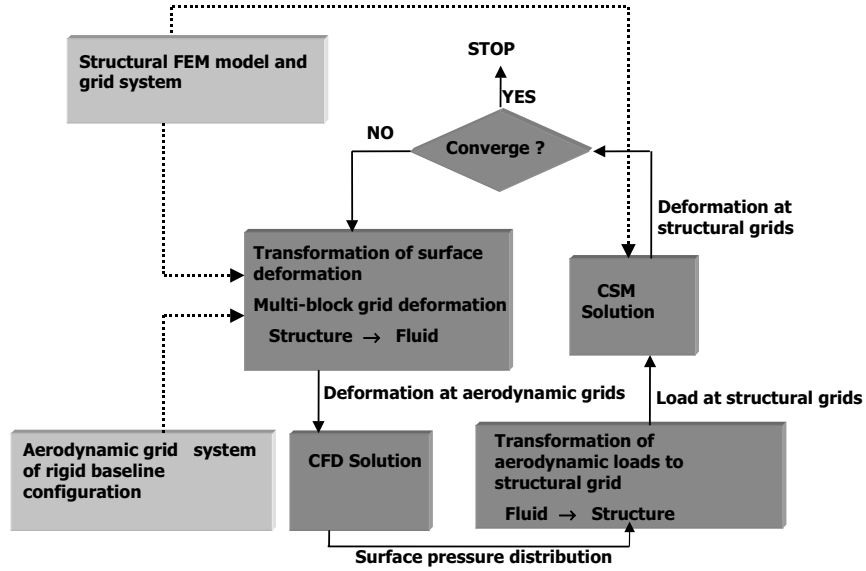
Fig. 3   Schematic diagram of the iterative process in static aeroelastic simulation
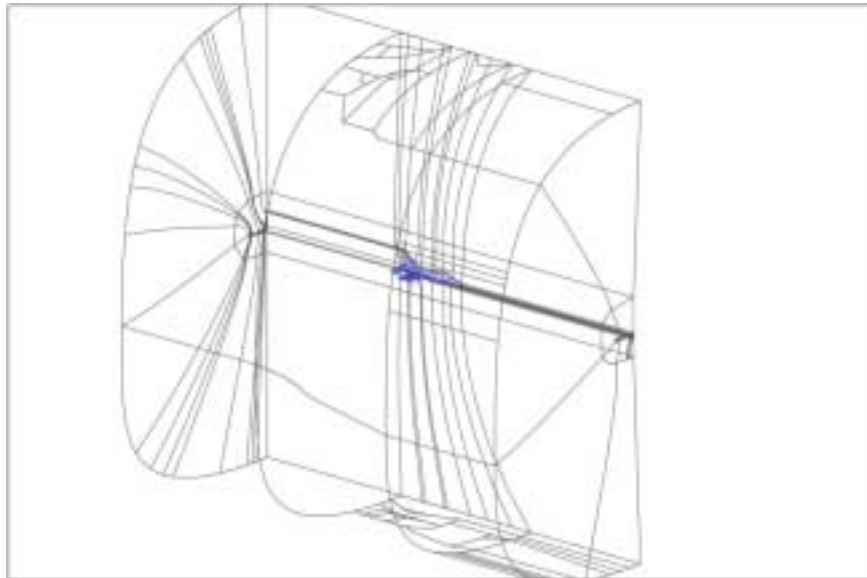
Fig. 4   Global view of the computational domain for the F-16 aircraft with tip missile
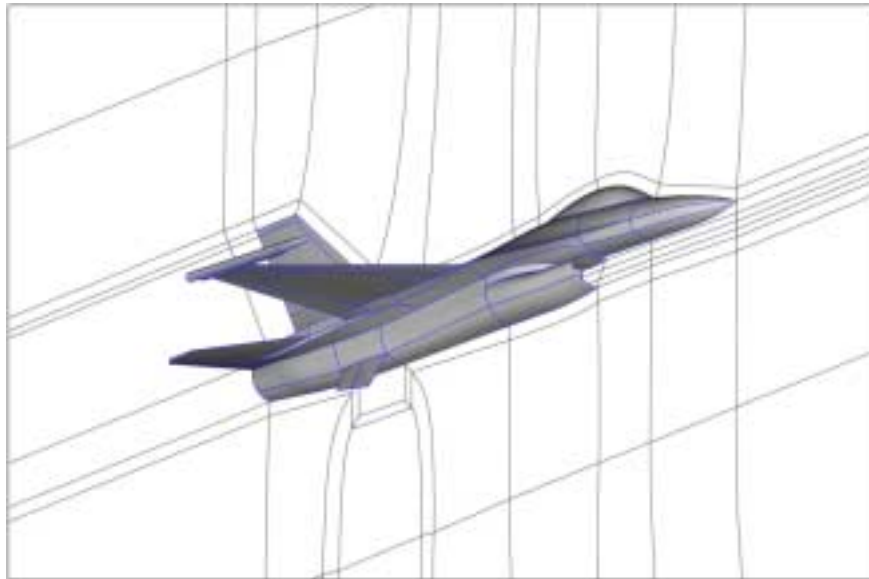
Fig. 5   Block boundaries close to the surface of F*-16 on the symmetry plane*
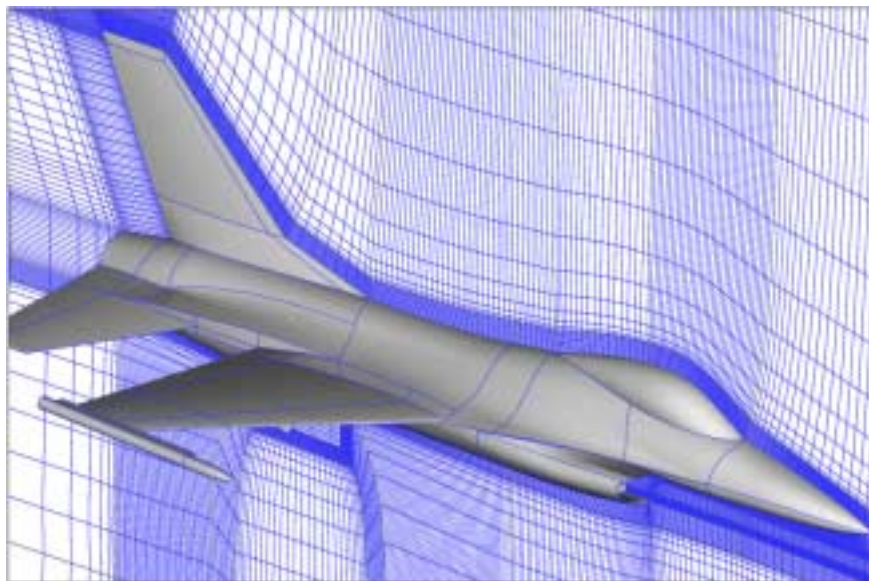
Fig. 6   Partial view of the grid on the symmetry plane for the analysis of F*-16 with tip missile*
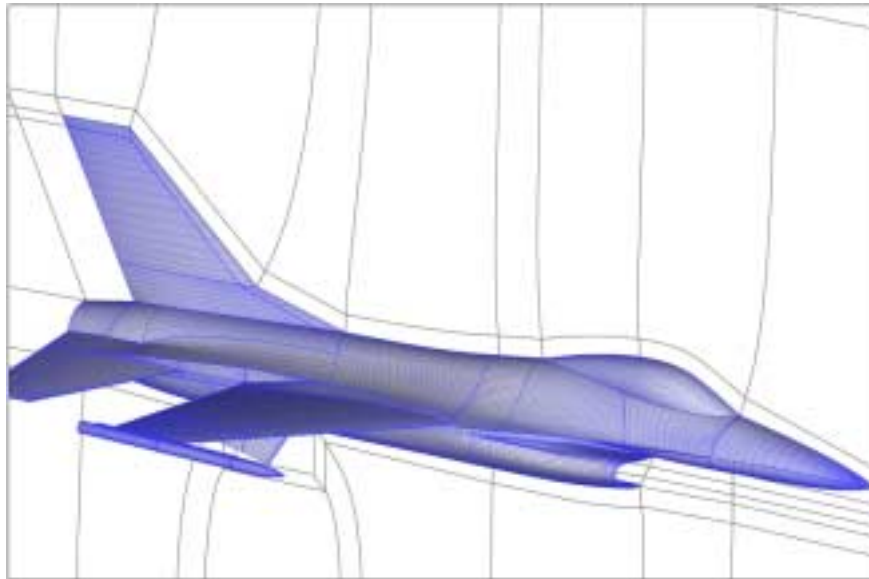
Fig. 7   Grid on the surface of F-16 *with tip missile*
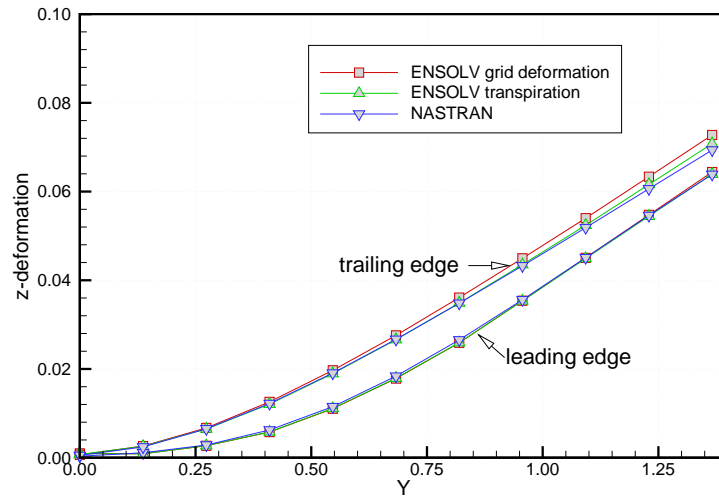
Fig. 8   Comparison of vertical deformation at the leading edge and trailing edge between NAS-
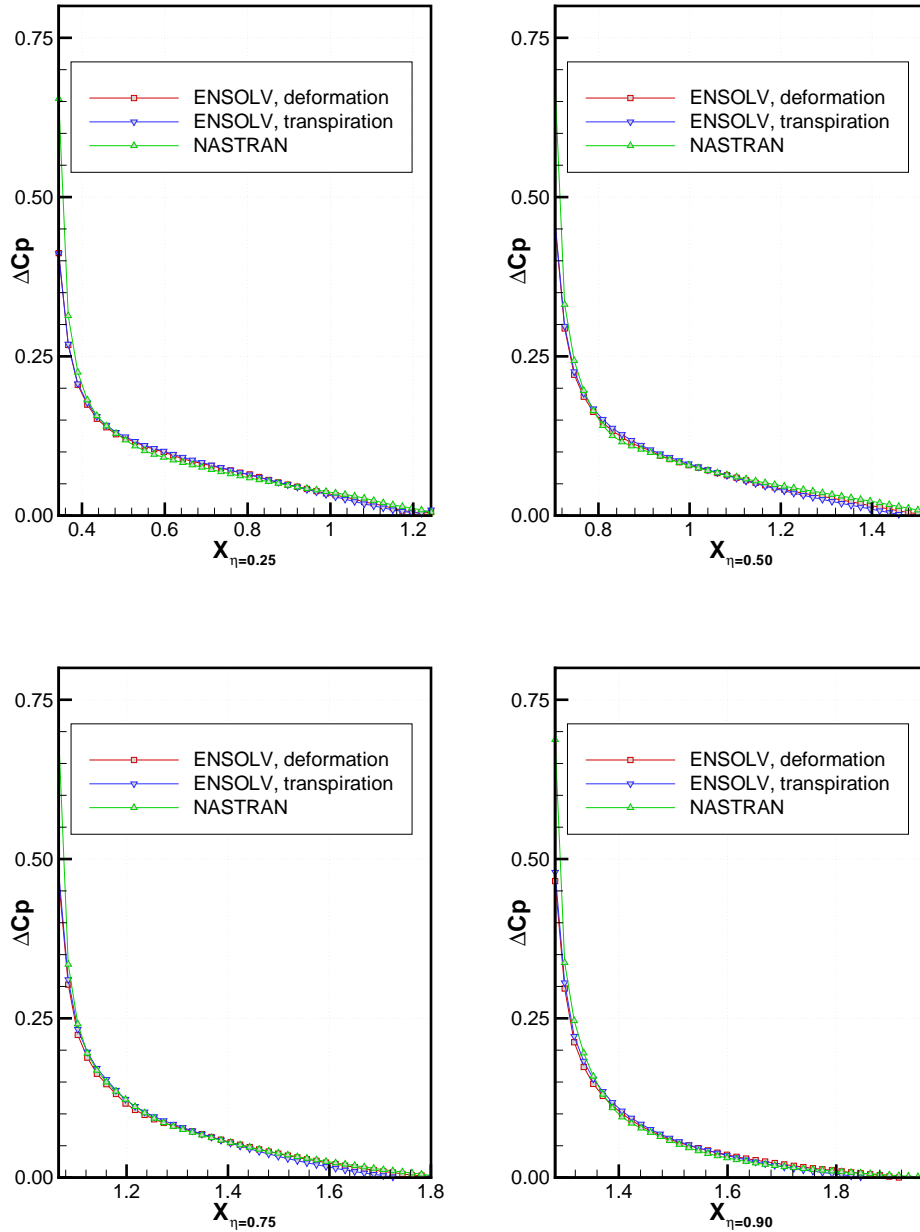TRAN *and* ENSOLV *(Euler),* M_∞*=0.45,* α*=2.00 degrees,* q_∞*=6372 Pa*
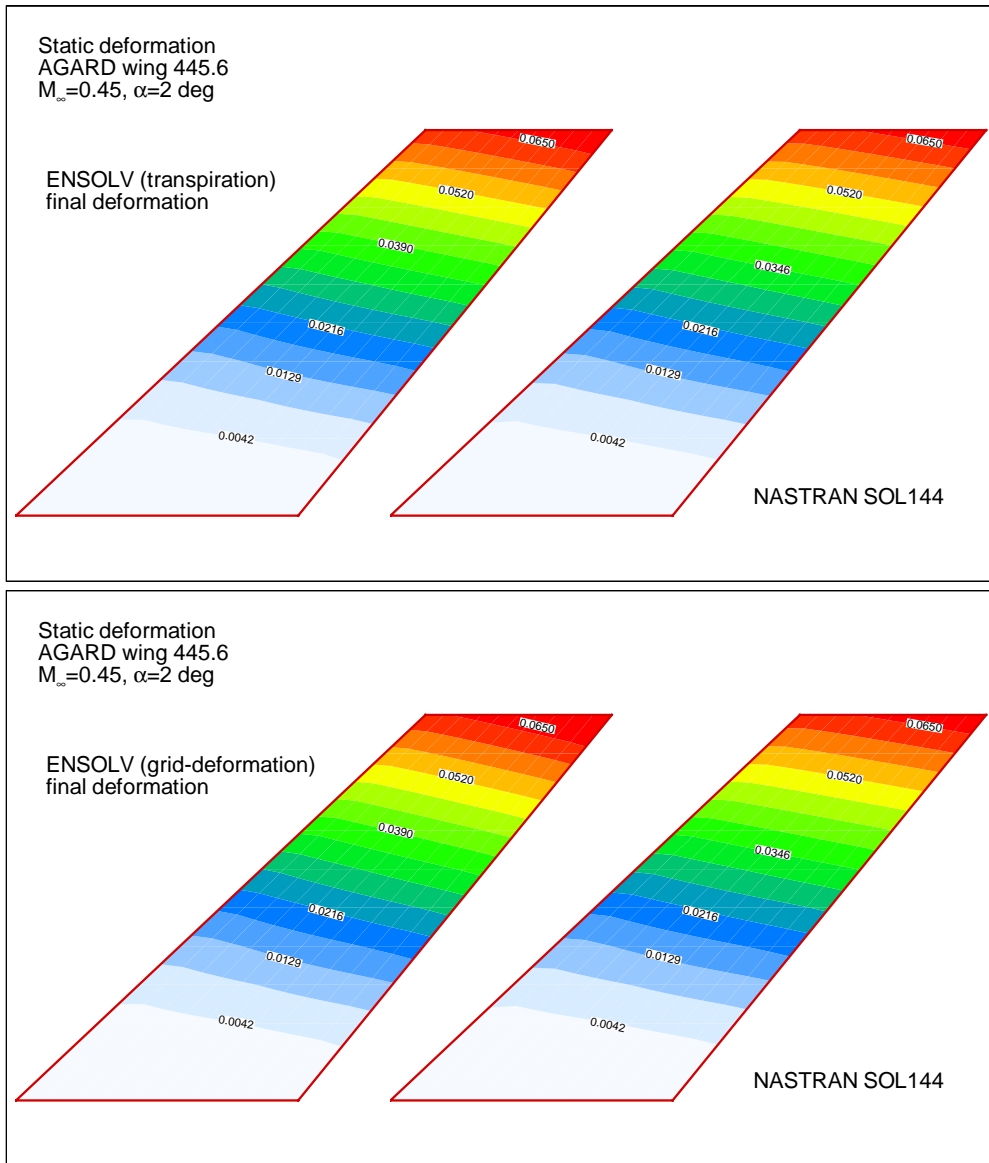
Fig. 9 Vertical-deformation contour of a restrained AGARD *wing obtained with* ENSOLV *using transpiration boundary condition and grid deformation approach and and* MSC.NASTRAN *at M_∞=0.45, α=2.00 degrees, q_∞=6372 Pa, Euler flow model*

Static deformation
AGARD wing 445.6
M_∞=0.45, α=2 deg

ENSOLV (transpiration)
lifting pressure (Cp$_L$-Cp$_U$)

NASTRAN SOL144
(Vortex-lattice)

Static deformation
AGARD wing 445.6
M_∞=0.45, α=2 deg

ENSOLV (grid–deformation)
lifting pressure (Cp$_L$-Cp$_U$)

NASTRAN SOL144
(Vortex-lattice)
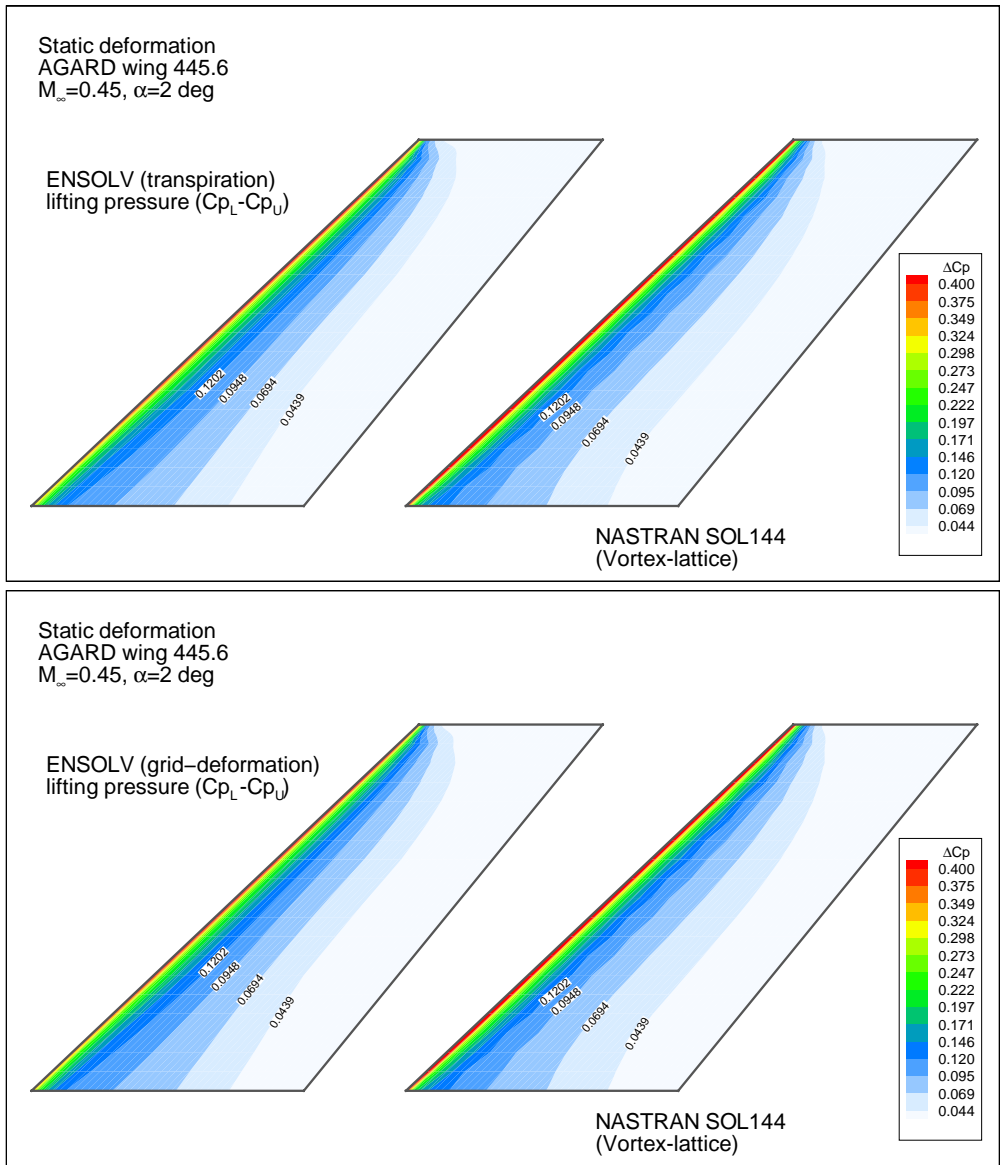
Fig. 10   *Lifting-pressure contour of a restrained* AGARD *wing obtained with* ENSOLV *using transpiration boundary condition and grid deformation approach and and* MSC.NASTRAN *at* M_∞=0.45, α=2.00 *degrees,* q_∞=6372 Pa, Euler flow model

Fig. 11   Sectional lifting-pressure contour of a restrained AGARD wing obtained with EN-SOLV using transpiration boundary condition and grid deformation approach and and MSC.NASTRAN at M_∞=0.45, α=2.00 degrees, q_∞=6372 Pa
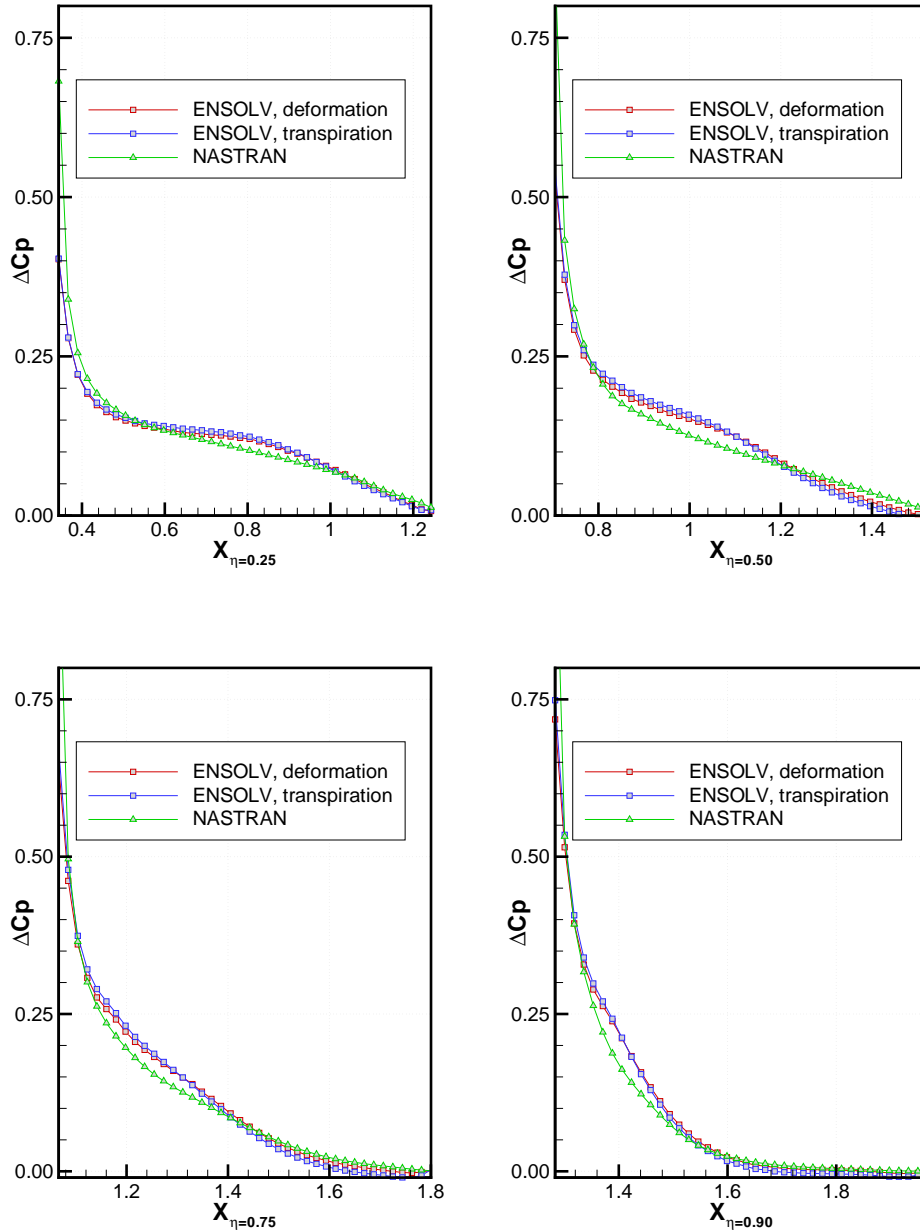
Fig. 12   Sectional lifting-pressure contour of a restrained AGARD wing obtained with EN-
SOLV using transpiration boundary condition and grid deformation approach and and
MSC.NASTRAN at M_∞=0.96, α=2.00 degrees, q_∞=3529 Pa
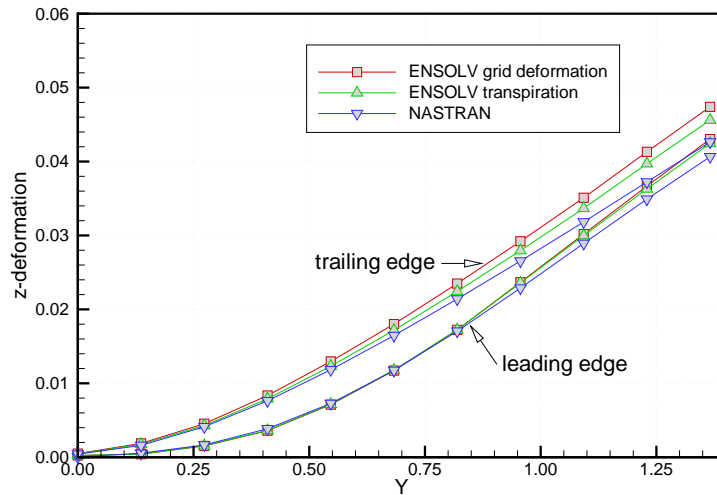
Fig. 13   *Comparison of the deformation in the z-direction at the leading edge and trailing edge between* NASTRAN *and* ENSOLV*, M_∞=0.96, α=2.00 degrees, q_∞=3529 Pa*
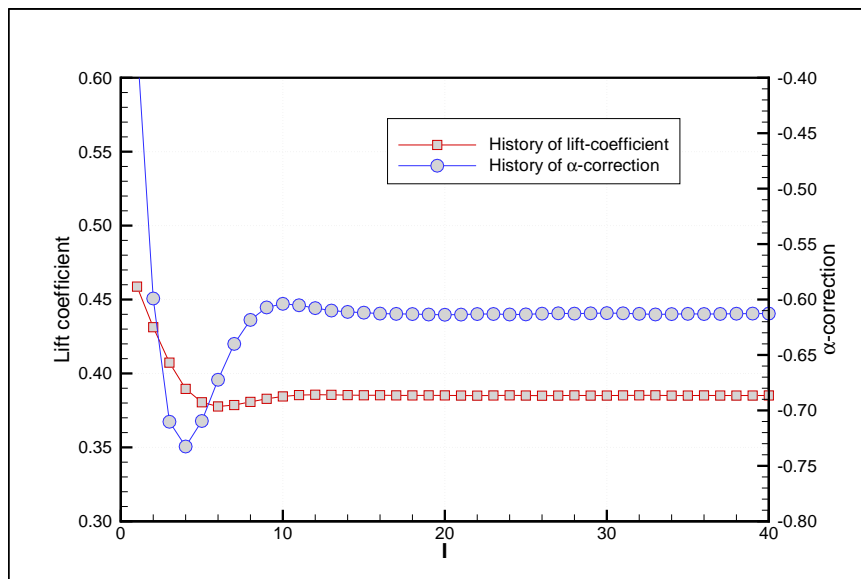
Fig. 14   *Convergence history of the lift coefficient and α correction of* F-16 *aircraft configuration with tip missiles for 5g pull-up maneuver flight at M_∞=0.90 and altitude 5,000 ft*
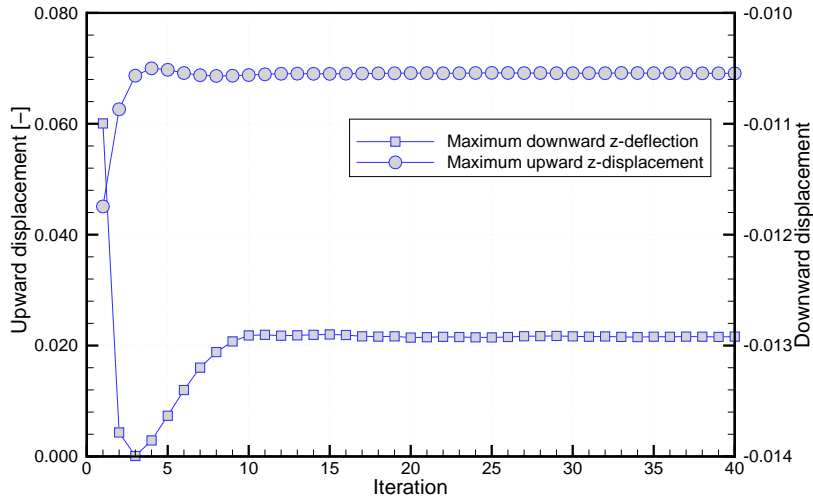
Fig. 15   Convergence history of the maximum upward and downward dimensionless deflection
of F-16 aircraft configuration with tip missiles for 5g pull-up maneuver flight at M_∞=0.90
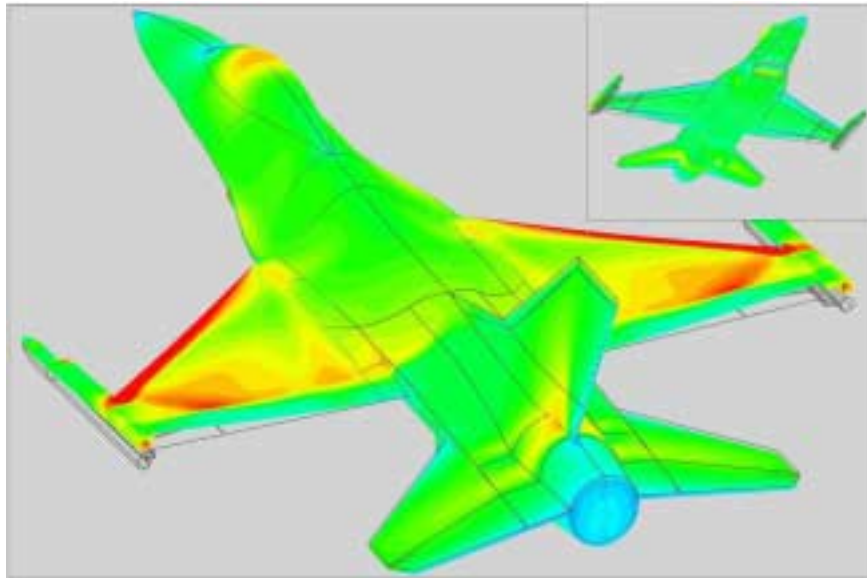and altitude 5,000 ft

Fig. 16   Surface pressure distribution of F-16 aircraft configuration with AMRAAM tip missiles
for 5g pull-up maneuver flight at M_∞=0.90 and altitude 5,000 ft calculated using con-
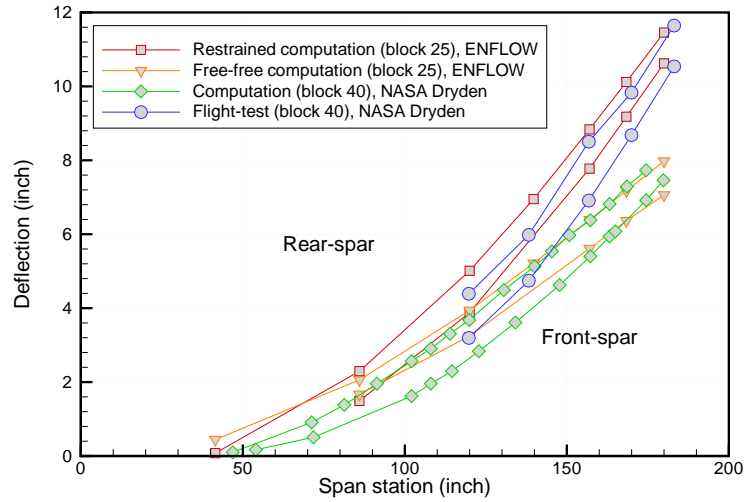strained model

Fig. 17   Spanwise distribution of the front and rear spars vertical deflection of F-16 aircraft con-
figuration with tip missiles for 5g pull-up maneuver flight at M_∞=0.90 and altitude 5,000
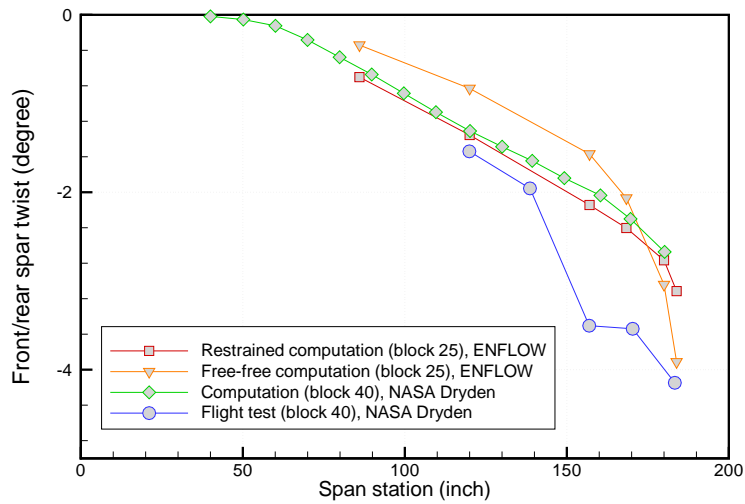*ft*

Fig. 18   Spanwise distribution of twist deformation of F-16 aircraft configuration with tip missiles
for 5g pull-up maneuver flight at M_∞=0.90 and altitude 5,000 f